crystals

MDPI

Article

Boron Nanotube Structure Explored by Evolutionary Computations

Tomasz Tarkowski [1] and Nevill Gonzalez Szwacki [2,*]

[1] Institute of Theoretical Physics, Faculty of Physics, University of Warsaw, Pasteura 5, PL-02093 Warsaw, Poland; tomasz.tarkowski@fuw.edu.pl
[2] Institute of Experimental Physics, Faculty of Physics, University of Warsaw, Pasteura 5, PL-02093 Warsaw, Poland
* Correspondence: gonz@fuw.edu.pl; Tel.: +48-22-5532797

Abstract: In this work, we explore the structure of single-wall boron nanotubes with large diameters (about 21 Å) and a broad range of surface densities of atoms. The computations are done using an evolutionary approach combined with a nearest-neighbors model Hamiltonian. For the most stable nanotubes, the number of 5-coordinated boron atoms is about 63% of the total number of atoms forming the nanotubes, whereas about 11% are boron vacancies. For hole densities smaller than about 0.22, the boron nanotubes exhibit randomly distributed hexagonal holes and are more stable than a flat stripe structure and a quasi-flat B_{36} cluster. For larger hole densities (>0.22), the boron nanotubes resemble porous tubular structures with hole sizes that depend on the surface densities of boron atoms.

Keywords: genetic algorithms; nanotubes; nanowires; model Hamiltonian

check for updates

Citation: Tarkowski, T.; Gonzalez Szwacki, N. Boron Nanotube Structure Explored by Evolutionary Computations. *Crystals* **2023**, *13*, 19. https://doi.org/10.3390/cryst13010019

Academic Editors: Yao Yao, Chaoyi Zhu and Songang Peng

Received: 30 November 2022
Revised: 15 December 2022
Accepted: 18 December 2022
Published: 23 December 2022

Copyright: © 2022 by the authors. Licensee MDPI, Basel, Switzerland. This article is an open access article distributed under the terms and conditions of the Creative Commons Attribution (CC BY) license (https://creativecommons.org/licenses/by/4.0/).

1. Introduction

Boron nanotubes (BNTs) have been synthesized for the first time in 2004 [1]. A magnesium-substituted mesoporous silica template (Mg-MCM-41) was applied by Ciuparu et al. [1] to prepare pure boron single-wall nanotubes at 870 °C with uniform diameters (36 ± 1 Å) using the mixture of BCl_3 and H_2 as gas sources. The authors attributed the Raman peaks at 210 cm^{-1} and between 300 and 500 cm^{-1} to typical tubular structures, where the first one (210 cm^{-1}) corresponds to the characteristic radial breathing mode. In 2010, Liu et al. [2] reported the first large-scale fabrication of single crystalline multilayered BNTs using boron (99.99%) and boron oxide powders (99.99%) as source materials. The as-synthesized BNTs had lengths of several micrometers and diameters in a range from 10 to 40 nm. The nanotubes were cataloged as multilayered single crystalline BNTs with an interlayer spacing of about 3.2 Å. Moreover, these nanotubes were experimentally proven to have metallic properties regardless of their chirality. The metallic behavior of BNTs makes them attractive in the design of novel electronic nanodevices such as field-effect transistors, light-emitting diodes, and field-emission displays, or for photosensitive device applications [3,4].

The experimental studies were preceded by several theoretical investigations, most often based on density functional theory (DFT). Quasiplanar [5,6], tubular [7,8], and convex and spherical [9] boron clusters have been computationally explored. Moreover, the existence of quasiplanar boron clusters [10,11] implies that boron fullerenes [12,13] and caped BNTs [14,15] may exist because larger quasiplanar or planar clusters will tend to remove dangling edge bonds by forming closed tubular or polyhedral structures.

Although some reports affirm that BNTs with diameters smaller than 1.7 nm [16,17] or 2 nm [18] show semiconducting behavior due to the band opening at the Fermi level through curvature-induced out-of-plane buckling of certain atoms, later calculations based on second-order Møller–Plesset perturbation theory [19] and dispersion-corrected DFT

calculations [20] showed that the surface buckling is more likely an artifact of standard DFT approaches.

Thus, BNTs are found to be metallic, and this property is independent of the diameter and chirality (armchair or zigzag) of the nanotube [21]. Moreover, there have been a lot of morphologies of BNTs in contrast to only one morphology of carbon nanotubes (CNTs) [22]. A more detailed description of the structure and properties of 1D-boron structures can be found in Refs. [4,23].

Crystal structure prediction (CSP) is a long-standing challenge in physical and materials sciences. Several methods have been applied for materials design [24,25]. Evolutionary algorithms, such as genetic algorithms (GAs) [25] that use human evolution mechanisms (such as crossover and mutation), have been used, for instance, to obtain the most stable structures of prototype nanotubes composed of particles interacting through a Lennard–Jones potential [26].

Boron two-dimensional structures [27] form foundations for BNTs since they can be obtained by "cutting out" adequate stripes and "gluing" them along the edges. Our previously developed methodology [28] based on the application of the floating-point representation is not the only possible strategy for the CSP of boron nanostructures. Alternatively, one can use binary (for monoatomic materials) or integer (for alloys) representations with a fixed crystal lattice. To obtain the total energy of the system, several approaches can be used. In our previous work, we used a genetic algorithm [29] combined with DFT to predict the structure of boron nanowires [28]. In this work, we will use a GA combined with a DFT-based nearest-neighbors model Hamiltonian to predict the structure of BNTs. We assume that the nanotubes have a perfect cylindrical shape and that their structure is closely related to one-atom-thick sheets of boron atoms arranged on a hexagonal lattice [27].

2. Computational Approach and Results of Simulations

2.1. Unit-Cell Definition

The information about the position of atoms and vacancies ("holes") on a hexagonal lattice wrapped cylindrically around a nanotube axis is encoded using a binary representation. The type of considered nanotubes is limited to an armchair (n, n) chirality as described in Ref. [8]. A cylindrical coordinate system can be conveniently used for the nanotube description. It is assumed that the nanotube has periodic boundary conditions (PBCs) in the z direction. The unit-cell size is described with two numbers $n_\phi, n_z \in \mathbb{N}_+$, where $n_\phi > 1$. The lattice constant (interatomic distance) of the unwrapped hexagonal layer is equal to a (to plot the BNTs in our figures, we have assumed $a = 1.675$ Å). The positions of atoms and vacancies are not encoded in the genotype but are specified by the following position vectors:

$$\vec{r}_i = \left(\frac{a\sqrt{6}}{4\sqrt{1-\cos(\pi/n_\phi)}}, \frac{\pi}{n_\phi} \cdot \left\lfloor \frac{i}{n_z} \right\rfloor, (i \bmod n_z) \cdot a + \begin{cases} 0 & \text{if } \lfloor i/n_z \rfloor \text{ is even} \\ a/2 & \text{otherwise} \end{cases} \right)_{(\rho,\phi,z)}. \quad (1)$$

The use of binary representation, $g = (x_i)_{i=0}^{c-1} \in \mathbb{B}^c$, where $c = 2n_\phi n_z$, justifies the way the vectors $\vec{r}_i$ are indexed (more details about indices is given in Appendix A). It also implies the number of atoms in the unit cell equal to $N_\mathrm{a} = \#\{i \in \iota_c \mid x_i\}$ and the number of vacancies equal to $N_\mathrm{v} = c - N_\mathrm{a}$.

The unit cell of the BNT is defined in terms of predicate theory. Predicate $Q \equiv Q_0 \wedge Q_1 \wedge Q_2$, where predicates Q_0, Q_1, and Q_2 state that atoms within the unit cell are connected, that there is an atomic neighborhood at the boundary of two unit cells along the nanotube axis, and that there is an atomic neighborhood at the unit cell boundary perpendicular to the circumference of the nanotube, respectively. The predicate Q is sufficient to ensure the nanotube connectivity and its closure at the circumference (see also Appendix A for a more precise formulation of the predicate Q). It does not restrict

any possible valid result of the structures that are equivalent by translational or rotational symmetry.

2.2. Fitness Function

The fitness function values are calculated using a nearest-neighbors model Hamiltonian. The optimization task consists in finding such a configuration of atoms and vacancies, which maximizes the fitness function—the binding energy per atom, E_b, calculated within the nearest-neighbors model Hamiltonian. In this model, E_b can be defined as:

$$E_b(n_1, n_2, n_3, n_4, n_5, n_6) = \frac{1}{N_a} \sum_{i=1}^{6} n_i e_i, \quad (2)$$

where n_i is the number of atoms in the unit cell with i nearest neighbors, while e_i is the E_b for a structure consisting of atoms having only i nearest neighbors (e.g., the two-atom molecule, single atomic chain, or a honeycomb structure, *hc*, for i equal to 1, 2, or 3, respectively). Obviously, the total number of atoms in the unit cell $N_a = \sum_{i=1}^{6} n_i$. The values of e_i are results of DFT calculations and are taken from our previous work [30]. They are equal to $e_1 = 1.7803$, $e_2 = 5.1787$, $e_3 = 5.6504$, $e_4 = 6.2522$, $e_5 = 6.5718$, and $e_6 = 6.5116$ in units of eV/atom. Since our model Hamiltonian includes only nearest-neighbors interactions and was developed for the case of a one-atom-thick layer of boron atoms [30,31], it does not take into account the curvature of the BNT. Therefore, the e_i parameters can be applied to nanotubes with large radii, where the effect of curvature on the properties of the nanotube is expected to be negligible.

In our previous work [30], we have obtained for 2D boron structures that, on average, their E_b values calculated using Equation (2) differ from those obtained using DFT calculations by 45 and 54 meV/atom for buckled and flat structures, respectively. These errors are, however, about two times smaller than the energy difference, $\Delta E_b^{DFT} = 91$ meV/atom, between E_b values of 6.603 and 6.512 meV/atom for the α-sheet and the buckled triangular (*bt*) sheet, respectively, and about twenty times smaller than the energy difference, $\Delta E_b^{DFT} = 953$ meV/atom, between E_b values of 6.603 and 5.650 meV/atom corresponding to the α and *hc* sheets, respectively [30]. Similar accuracy may be expected for the E_b values predicted using Equation (2) for BNTs, at least for those nanotubes with large diameters (20 Å and above).

In the case of carbon, the elastic properties of the nanotubes do not depend on the diameter at approximately 18 Å [32] . The same is true for electronic properties such as the energy gap [33]. Making the assumption that the pure boron case situation is the same, $n_\phi = 23$ is taken, which corresponds to $\rho \approx 10.628$ Å. This gives the size of the potential solution space (described by a general formula of $2^{2n_\phi n_z}$) equal to $2^{46 n_z}$.

The Bernoulli $B(1, 0.5)$ probability distribution ($B(n, p)$ is a discrete probability distribution, where the Bernoulli random variable n can have only 0 or 1 as the outcome values, p is the probability of success ($n = 1$), and $1 - p$ is the probability of failure ($n = 0$)) was chosen for the creation of the first generation of nanotubes, and genotypes not satisfying the predicate Q were rejected. A one-point recombination with bit-flipping mutation ($p = 1/c$) applied stochastically with probabilities equal to $p_r = p_m = 0.5$ is employed during the evolution.

The generation size μ is set to $4n_\phi n_z$ while parent multiset size $2k = 2n_\phi n_z$. Stochastic universal sampling (SUS) with linear ranking selection ($s = 2$) is used for the parent selection and the selection of the next-generation mechanisms. The genetic search is terminated after reaching a *plateau* for the fitness function or, more precisely, when after 100 generations the fitness function maximum has not improved by $\Delta E = 1$ meV.

Some of the obtained nanotubes can be equivalent through rotations around the z-axis and translations along this axis. There is a relationship between natural numbers and the above-defined nanotubes. Encoding $g \in \mathbb{B}^{2n_\phi n_z}$ corresponds to certain number $n = \sum_{i=0}^{2n_\phi n_z - 1} 2^i x_i$, where $\mathbb{B} \ni \text{true} \equiv 1 \in \mathbb{N}$ and $\mathbb{B} \ni \text{false} \equiv 0 \in \mathbb{N}$. There are classes of

abstractions of natural numbers regarding rotations around the z-axis (nanotube axis) and translations along this axis, which form equivariant nanotubes. Rotations and translations in the set $\iota_{2n_\phi n_z}$ can be defined as follows:

$$R^{\Delta n_\phi}_{n_\phi,n_z}(n) = n',\ x'_{(i+2\Delta n_\phi n_z) \bmod 2n_\phi n_z} = x_i, \tag{3}$$

$$T^{\Delta n_z}_{n_\phi,n_z}(n) = n',\ x'_{((i+\Delta n_z) \bmod n_z)+\lfloor i/n_z \rfloor n_z} = x_i, \tag{4}$$

where $\Delta n_\phi, \Delta n_z \in \mathbb{Z}$. The following identities hold:

$$R^{n_\phi}_{n_\phi,n_z} = \mathrm{id}, \tag{5}$$

$$T^{n_z}_{n_\phi,n_z} = \mathrm{id}, \tag{6}$$

$$R^{\Delta n_\phi}_{n_\phi,n_z} = \left(R^1_{n_\phi,n_z}\right)^{\Delta n_\phi}, \tag{7}$$

$$T^{\Delta n_z}_{n_\phi,n_z} = \left(T^1_{n_\phi,n_z}\right)^{\Delta n_z}, \tag{8}$$

$$R^{-1}_{n_\phi,n_z} = R^{n_\phi-1}_{n_\phi,n_z}, \tag{9}$$

$$T^{-1}_{n_\phi,n_z} = T^{n_z-1}_{n_\phi,n_z}. \tag{10}$$

It may also turn out that the nanotube obtained as a result of evolution has a shorter elementary unit cell along $\hat{e}_z$ than would result from the n_z value. This occurs if and only if the maximum divisor d_{n_z} of the number n_z, for which the condition

$$T^{n_z/d_{n_z}}_{n_\phi,n_z}(n) = n, \tag{11}$$

is satisfied for n representing a given nanotube, is greater than 1. If maximum divisor d_{n_ϕ} of n_ϕ, for which the analogous condition

$$R^{n_\phi/d_{n_\phi}}_{n_\phi,n_z}(n) = n \tag{12}$$

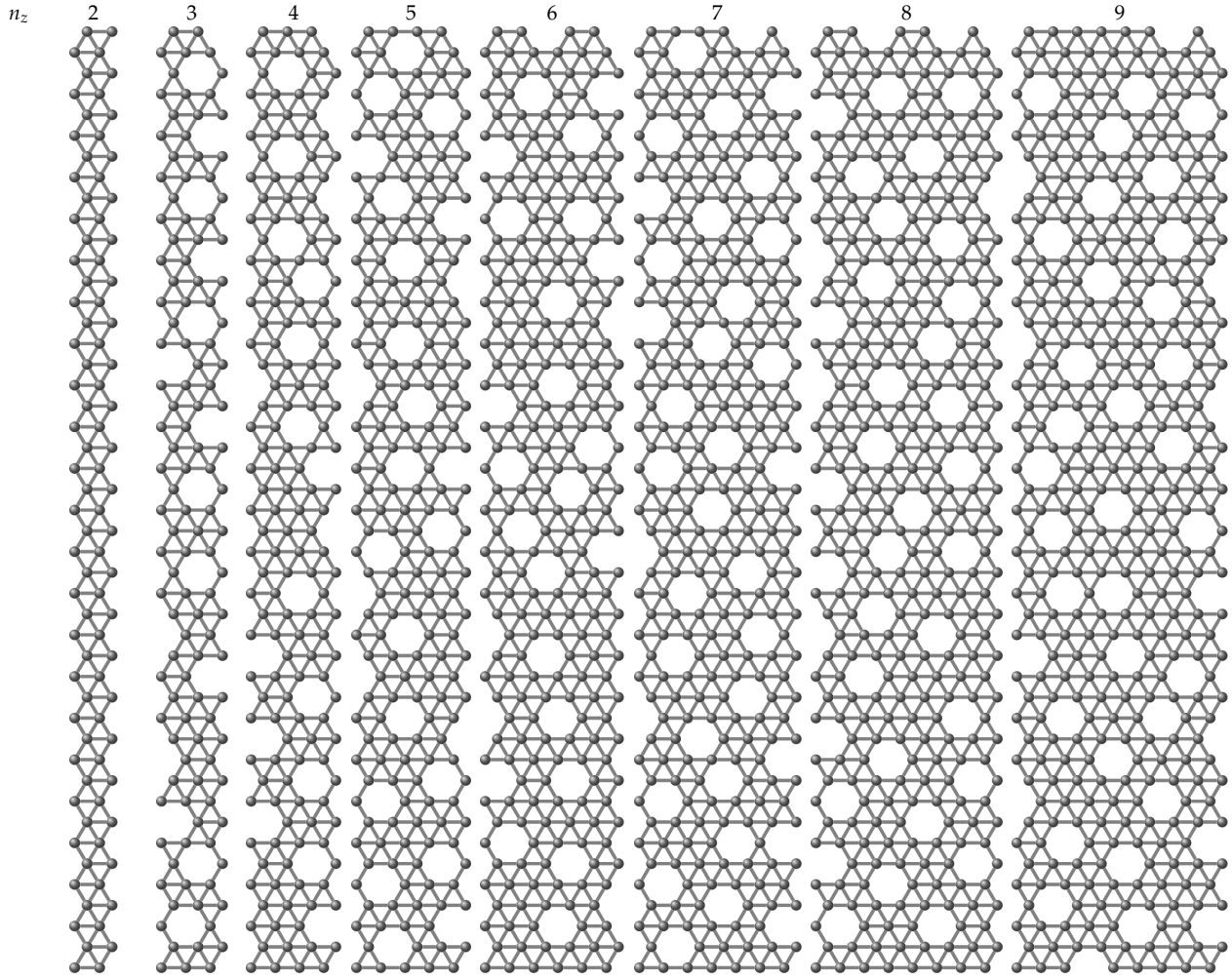
is met, is greater than 1 then the nanotube has a nontrivial rotational symmetry about the axis of the tube. The values of d_{n_z} and d_{n_ϕ} are assumed to be the maximum values satisfying the conditions given by Equations (11) and (12), respectively.

2.3. Results of Simulations

The most stable evolutionary obtained nanotubes are labeled as τ_{n_ϕ,n_z}. The computational complexity for a given value of n_ϕ grows exponentially with the unit cell length n_z. For $n_\phi = 23$, under the assumption that a single structure has proceeded for 10 µs even for $n_z = 2$ with sequential computations, the time five orders of magnitude longer than the Universe age [34] is needed to check all possible potential solutions. The application of a genetic algorithm is therefore advisable.

The most energetically favorable nanotubes are presented in Figure 1. The evolutionary obtained structure $\tau_{23,2}$ is the case of a fully filled with boron atoms lattice. The removal of any atom from a fully filled lattice is energetically favorable since it raises the number of 5-coordinated atoms (raise of the beneficial value of n_5). The density of vacancies cannot be too high since the situation with holes that are too close to each other may be detrimental for E_b as it may increase the number of 4-coordinated atoms (raise of the detrimental value of n_4). Looking at Figure 1, we may conclude that, in general, the most energetically favorable are those nanotubes for which the boron holes are separated by fragments of the boron double chain (BDC) or boron triple chain (BTC). Less favorable are those situations in which the holes are next to each other. The highest E_b value in our simulation belongs to the $\tau_{23,8}$ nanotube (6.55108 eV/atom) after which the $\tau_{23,4}$ nanotube (6.55102 eV/atom) is located. Recalling that DFT calculation precision is of the order of 1 meV/atom [35], one

can assume that both nanotubes have equal E_b values (within our model). In Figure 1, we also show the time taken to obtain the results, within our approach, for the most stable examples of BNTs for a given value of n_z. Although our methodology is relatively simple, the time taken to obtain, for instance, $\tau_{23,9}$ exceeds 6 days. This tells us that computations that would involve more accurate fitness functions may require prohibitive computational times.



	$\tau_{23,2}$	$\tau_{23,3}$	$\tau_{23,4}$	$\tau_{23,5}$	$\tau_{23,6}$	$\tau_{23,7}$	$\tau_{23,8}$	$\tau_{23,9}$
E_b	6.512	6.547	6.551	6.550	6.548	6.550	6.551	6.548
c	92	138	184	230	276	322	368	414
N_a	92	122	164	203	247	285	327	370
N_v	0	16	20	27	29	37	41	44
n_4	0	4	2	5	4	6	5	6
n_5	0	88	116	152	166	210	236	252
n_6	92	30	46	46	77	69	86	112
d_{n_ϕ}	23	1	1	1	1	1	1	1
d_{n_z}	2	1	1	1	1	1	1	1
Δt	2:20:42:33	0:04:43:57	0:03:32:40	0:05:33:33	0:11:15:37	1:00:12:09	2:13:54:34	6:12:22:56

Figure 1. Fragments of boron sheets that, if rolled into nanotubes, give the most stable BNTs that were obtained in our evolutionary computations. The unit cell of each BNT is defined by two parameters (n_ϕ, n_z), where $n_\phi = 23$ and n_z is specified above each stripe. Below each stripe, several parameters are listed that characterize each nanotube (see text). The binding energy per atom, E_b, is given in units of eV/atom. The holes in the nanotubes are vacancies in the hexagonal structure wrapped on a cylinder to form a nanotube. The density of holes can be calculated using the formula $\eta = N_v/c$, where $c = N_a + N_v$. The values of the calculation time, Δt, are presented using the days:hours:minutes:seconds format. One evolutionary process was performed on one logical thread of a multithreaded CPU [36]. The unit cell of the $\tau_{23,8}$ BNT, is shown in the inset of Figure 2.

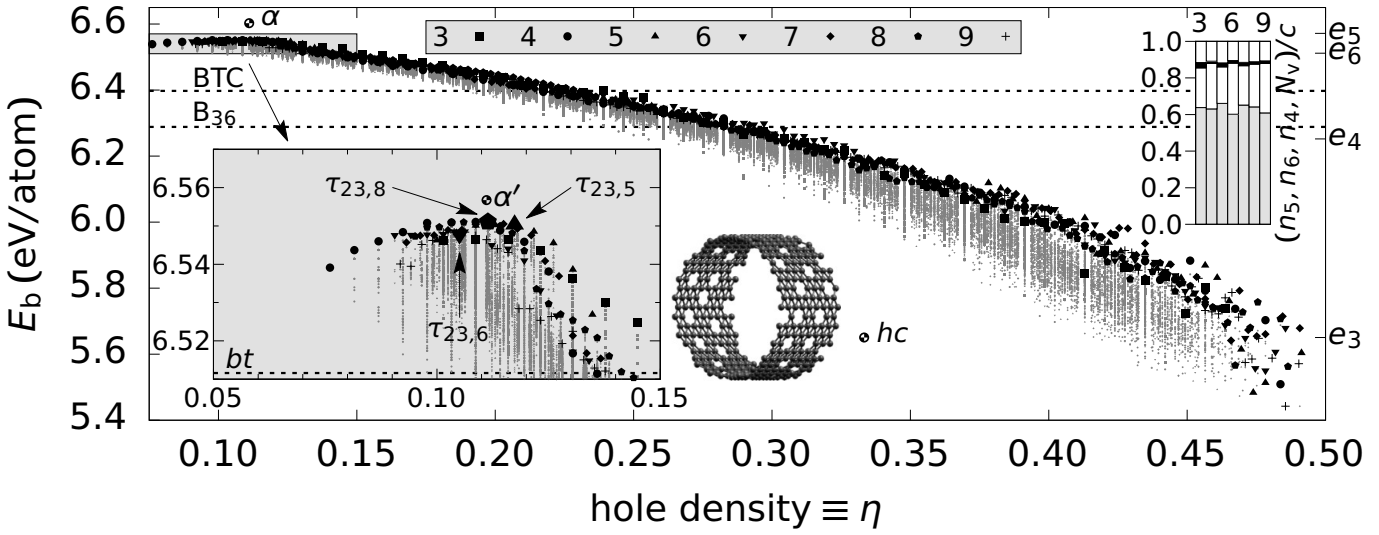


Figure 2. Binding energy per atom, E_b, calculated using Equation (2) as a function of hole density, η. The data points in black correspond to BNTs with maximum values of E_b obtained for a given n_z parameter ($n_\phi = 23$) and shown with a different label. The data points in gray show the full evolution and correspond to nonoptimal BNTs. The $n_z \in \{3, 4, \ldots, 9\}$ to label correspondence is provided above the data points. Shown are also data points for the *hc* and α sheets (with E_b^{DFT} values equal to 5.650 and 6.603 eV/atom, respectively [30]), as well as energy levels (dotted lines) associated with the BTC and B_{36} structures (with E_b^{DFT} values equal to 6.397 and 6.288 eV/atom, respectively [30]). The inset on the left (with gray background) shows an enlarged view of a fragment of the main picture. The data point labeled as α' corresponds to the α-sheet with $E_b = 6.557$ eV/atom calculated using Equation (2). The energy level corresponding to $E_b^{DFT} = 6.512$ eV/atom [30] of the *bt*-sheet is also shown. The histogram on the right presents (from bottom) the values of n_5/c (gray), n_6/c (white), n_4/c (black), and N_v/c (white) for τ_{23,n_z} nanotubes. In the center, the unit cell of the $\tau_{23,8}$ nanotube is shown.

The relation between E_b and hole density, $\eta = N_v/c$, is presented in Figure 2. If one were to draw a curve that represents the average of the E_b values shown in Figure 2 as a function of hole density, the maximum of this curve would correspond to the hole density of $1/9 = 0.111$, which is the hole density of the α-sheet [27] (the optimal flat neutral boron 2D structure). The histogram shown in the inset of Figure 2 presents the number of 4-, 5-, and 6-coordinated boron atoms as well as boron vacancies relative to the total number of possible boron sites ($c = N_a + N_v$) for the most stable BNTs. The average over the 7 relevant cases studied ($n_z \in \{3, 4, \ldots, 9\}$) gives us that the number of 4-, 5-, and 6-coordinated boron atoms is about 2%, 63%, and 24%, respectively, of the total number of atoms forming the nanotubes, whereas about 11% are boron vacancies. This gives us a very interesting result that more than 85% of the boron atoms in BNTs with the largest E_b values are highly coordinated atoms.

In Figure 3, we show three examples of BNTs for three substantially different hole densities η equal to 0, 0.122, and 0.239. For hole densities smaller than about 0.22, the boron nanotubes exhibit randomly distributed hexagonal holes and are more stable than a flat stripe structure and a quasi-flat B_{36} cluster (see Figure 2). For larger hole densities (>0.22), the boron nanotubes resemble porous tubular structures with hole sizes that depend on the surface densities of boron atoms. Finally, it should be noted that almost all of the studied BNTs in this work have E_b values between 5.65 eV/atom and 6.60 eV/atom, which correspond to E_b of the *hc* and α sheets, respectively [30].

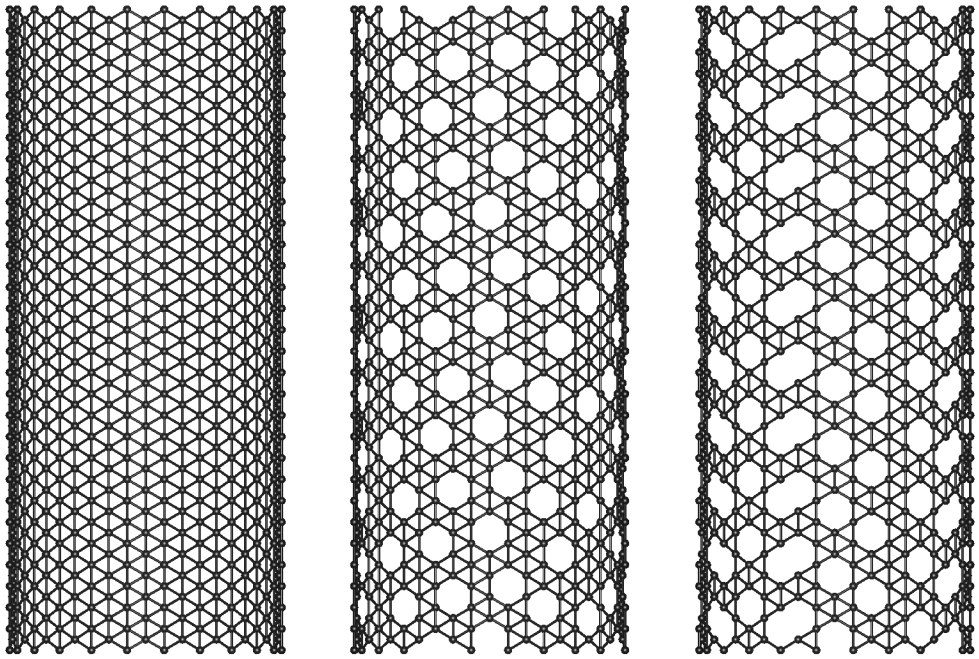


Figure 3. Examples of BNTs with three different hole densities. For each nanotube, the n_ϕ and n_z parameters, which describe the unit-cell size, are provided. To obtain the same height of the nanotubes, the 2, 5, and 3 values of n_z are multiplied by 15, 6, and 10, respectively (for a total height of 50.25 Å). The binding energy, E_b, and hole density, η, are also given.

3. Summary

In conclusion, we have presented an adaptation of the genetic algorithm for the structure prediction of tubular BNTs in a broad range of possible hole densities. The evolution of the structures is achieved using a binary representation and a fitness function calculated using a model Hamiltonian. For the most stable BNTs, the number of 5-coordinated boron atoms is about 63% of the total number of atoms forming the nanotubes, whereas about 11% are boron vacancies. Moreover, more than 85% of the boron atoms in BNTs with the largest E_b values are 5- and 6-coordinated atoms. For hole densities smaller than about 0.22, the BNTs exhibit randomly distributed hexagonal holes and are more stable than the BTC structure and a quasi-flat B_{36} cluster. For larger hole densities ($>$0.22), the BNTs resemble porous tubular structures with hole sizes that depend on the surface densities of boron atoms. These prototype genetic algorithm calculations may serve for the exploration of the structure of nanotubes based on a mixture of boron and other atoms (e.g., carbon and/or nitrogen).

In addition, we can learn from our approach that the central parameters that determine the structure of BNTs are the coordination numbers of the constituent atoms. Each atom that has a given coordination number contributes with a given energy to E_b, and from the balance between different contributions we obtain porous BNTs with regularly distributed holes. We do not observe the fragmentation of the nanotubes for any of the studied hole densities. This remarkable result should attract the attention of experimentalists seeking to extend the effort of synthesizing BNTs to structures with a broader range of hole densities (from 0 to up to about 0.3), which would certainly extend a range of possible applications of BNTs.

Author Contributions: Conceptualization, T.T. and N.G.S.; methodology, T.T.; software, T.T.; validation, T.T.; investigation, T.T. and N.G.S.; writing—original draft preparation, T.T.; writing—review & editing, N.G.S.; visualization, T.T.; supervision, N.G.S. All authors have read and agreed to the published version of the manuscript.

Funding: This work is a result of the projects funded by the National Science Centre of Poland under grant numbers UMO-2013/11/B/ST3/04273 and UMO-2016/23/B/ST3/03575.

Data Availability Statement: The data reported in this study can be available by request from the authors.

Conflicts of Interest: The authors declare no conflict of interest.

Appendix A

Let us define some helper functions describing the indices of six lattice sites (atoms and vacancies) that are neighbors of a given site of the wrapped hexagonal lattice. If a given lattice site has an index i, then the sites up left, up right, left, right, down left, and down right have indices equal to $u_l^*(i)$, $u_r^*(i)$, $l^*(i)$, $r^*(i)$, $d_l^*(i)$, and $d_r^*(i)$, respectively. Those functions are formulated in the following way:

$$u_l^* = l^* \circ u_r^*, \tag{A1}$$

$$u_r^*(i) = (i + n_z + o^*(i)) \bmod 2n_\phi n_z, \tag{A2}$$

$$l^*(i) = i - 1 + \begin{cases} 0 & \text{if } i \bmod n_z \neq 0 \\ n_z & \text{otherwise} \end{cases}, \tag{A3}$$

$$r^*(i) = i + 1 - \begin{cases} 0 & \text{if } i \bmod n_z \neq n_z - 1 \\ n_z & \text{otherwise} \end{cases}, \tag{A4}$$

$$d_l^* = l^* \circ d_r^*, \tag{A5}$$

$$d_r^*(i) = (i - n_z + o^*(i)) \bmod 2n_\phi n_z, \tag{A6}$$

where the offset o^* is defined as:

$$o^*(i) = \begin{cases} 0 & \text{if } \lfloor i/n_z \rfloor \text{ is even} \\ 1 & \text{if } \lfloor i/n_z \rfloor \text{ is odd} \wedge i \bmod n_z \neq n_z - 1 \\ 1 - n_z & \text{otherwise} \end{cases}. \tag{A7}$$

Let $\mathrm{id}(i) = i$. The following relations hold:

$$u_l^* = d_r^{*-1}, \tag{A8}$$

$$l^* = r^{*-1}, \tag{A9}$$

$$d_l^* = u_r^{*-1}, \tag{A10}$$

$$u_l^{*2n_\phi} = d_l^{*2n_\phi} = l^{*2}, \tag{A11}$$

$$l^{*n_z} = r^{*n_z} = \mathrm{id}, \tag{A12}$$

$$u_r^{*2n_\phi} = d_r^{*2n_\phi} = r^{*2}. \tag{A13}$$

Functions u_l^*, u_r^*, r^*, and d_r^* are used to ensure neighborhood along the nanotube axis direction and at its circumference. To ensure connectivity, an additional set of functions is needed. These functions do not reflect PBCs. If a given atom or vacancy does not possess a suitable neighbor (i.e., it lies at the unit cell boundary), then the appropriate function returns an unchanged index:

$$u_l(i) = i + \begin{cases} 0 & \text{if } \lfloor i/n_z \rfloor = 2n_\phi - 1 \\ 0 & \text{if } \lfloor i/n_z \rfloor \text{ is even} \wedge i \bmod n_z = 0 \\ n_z - 1 & \text{if } \lfloor i/n_z \rfloor \text{ is even} \wedge i \bmod n_z \neq 0 \\ n_z & \text{otherwise} \end{cases}, \tag{A14}$$

$$u_r(i) = i + \begin{cases} 0 & \text{if } \lfloor i/n_z \rfloor = 2n_\phi - 1 \\ 0 & \text{if } \lfloor i/n_z \rfloor \text{ odd} \wedge i \bmod n_z = n_z - 1 \\ n_z + 1 & \text{if } \lfloor i/n_z \rfloor \text{ odd} \wedge i \bmod n_z \neq n_z - 1 \\ n_z & \text{otherwise} \end{cases}, \tag{A15}$$

$$l(i) = i - \begin{cases} 1 & \text{if } i \bmod n_z \neq 0 \\ 0 & \text{otherwise} \end{cases}, \tag{A16}$$

$$r(i) = i + \begin{cases} 1 & \text{if } i \bmod n_z \neq n_z - 1 \\ 0 & \text{otherwise} \end{cases}, \tag{A17}$$

$$d_l(i) = i - \begin{cases} 0 & \text{if } \lfloor i/n_z \rfloor = 0 \\ 0 & \text{if } \lfloor i/n_z \rfloor \text{ is even} \wedge i \bmod n_z = 0 \\ (n_z + 1) & \text{if } \lfloor i/n_z \rfloor \text{ is even} \wedge i \bmod n_z \neq 0 \\ n_z & \text{otherwise} \end{cases}, \tag{A18}$$

$$d_r(i) = i - \begin{cases} 0 & \text{if } \lfloor i/n_z \rfloor = 0 \\ 0 & \text{if } \lfloor i/n_z \rfloor \text{ is odd} \wedge i \bmod n_z = n_z - 1 \\ (n_z - 1) & \text{if } \lfloor i/n_z \rfloor \text{ is odd} \wedge i \bmod n_z \neq n_z - 1 \\ n_z & \text{otherwise} \end{cases}. \tag{A19}$$

To formulate the Q predicate, elements of graph theory are used. The set of *vertices*, V, consists of indices of all atoms taken from a single unit cell:

$$V = \left\{ i \in \iota_{2n_\phi n_z} \mid x_i \right\}, \tag{A20}$$

while the set of (undirected) *edges*, E, whose vertices fulfill the neighborhood condition in the nanotube's fragment (unit cell) without PBCs, is now defined as:

$$E = \{\{i, j\} \subseteq V \mid j \in \{u_l(i), u_r(i), l(i), r(i), d_l(i), d_r(i)\} \setminus \{i\}\}. \tag{A21}$$

By taking a pair of both objects, one obtains *graph* $H = (V, E)$. The Q predicate is defined as $Q \equiv Q_0 \wedge Q_1 \wedge Q_2$, where:

$$Q_0 \equiv \omega(H) = 1, \tag{A22}$$

$$Q_1 \equiv \Big(\exists i \in \iota_{2n_\phi n_z} \colon \lfloor i/n_z \rfloor \text{ is odd} \wedge i \bmod n_z = n_z - 1 \wedge x_i \wedge (x_{u_r^*(i)} \vee x_{d_r^*(i)})\Big) \vee \Big(\exists i \in \iota_{2n_\phi n_z} \colon \lfloor i/n_z \rfloor \text{ is even} \wedge i \bmod n_z = n_z - 1 \wedge x_i \wedge x_{r^*(i)}\Big), \tag{A23}$$

$$Q_2 \equiv \Big(\exists i \in \iota_{2n_\phi n_z} \colon \lfloor i/n_z \rfloor = 2n_\phi - 1 \wedge x_i \wedge (x_{u_l^*(i)} \vee x_{u_r^*(i)})\Big), \tag{A24}$$

and $\omega(H)$ is the number of *connected components* of graph H.

References

1. Ciuparu, D.; Klie, R.F.; Zhu, Y.; Pfefferle, L. Synthesis of Pure Boron Single-Wall Nanotubes. *J. Phys. Chem. B* **2004**, *108*, 3967–3969. [CrossRef]
2. Liu, F.; Shen, C.; Su, Z.; Ding, X.; Deng, S.; Chen, J.; Xu, N.; Gao, H. Metal-like single crystalline boron nanotubes: Synthesis and in situ study on electric transport and field emission properties. *J. Mater. Chem.* **2010**, *20*, 2197. [CrossRef]
3. Tian, J.; Xu, Z.; Shen, C.; Liu, F.; Xu, N.; Gao, H.J. One-dimensional boron nanostructures: Prediction, synthesis, characterizations, and applications. *Nanoscale* **2010**, *2*, 1375. [CrossRef] [PubMed]
4. Tian, Y.; Guo, Z.; Zhang, T.; Lin, H.; Li, Z.; Chen, J.; Deng, S.; Liu, F. Inorganic Boron-Based Nanostructures: Synthesis, Optoelectronic Properties, and Prospective Applications. *Nanomaterials* **2019**, *9*, 538. [CrossRef] [PubMed]

5. Boustani, I. New Convex and Spherical Structures of Bare Boron Clusters. *J. Solid State Chem.* **1997**, *133*, 182–189. [CrossRef]
6. Boustani, I. Systematic *ab initio* investigation of bare boron clusters: Determination of the geometry and electronic structures of B_n $(n = 2-14)$. *Phys. Rev. B* **1997**, *55*, 16426–16438. [CrossRef]
7. Boustani, I.; Quandt, A. Nanotubules of bare boron clusters: *Ab initio* and density functional study. *Europhys. Lett. (Epl)* **1997**, *39*, 527–532. [CrossRef]
8. Gindulytė, A.; Lipscomb, W.N.; Massa, L. Proposed Boron Nanotubes. *Inorg. Chem.* **1998**, *37*, 6544–6545. [CrossRef]
9. Boustani, I.; Rubio, A.; Alonso, J.A. Ab initio study of B_{32} clusters: Competition between spherical, quasiplanar and tubular isomers. *Chem. Phys. Lett.* **1999**, *311*, 21–28. [CrossRef]
10. Kiran, B.; Bulusu, S.; Zhai, H.J.; Yoo, S.; Zeng, X.C.; Wang, L.S. Planar-to-tubular structural transition in boron clusters: B_{20} as the embryo of single-walled boron nanotubes. *Proc. Natl. Acad. Sci. USA* **2005**, *102*, 961–964. [CrossRef]
11. Piazza, Z.A.; Hu, H.S.; Li, W.L.; Zhao, Y.F.; Li, J.; Wang, L.S. Planar hexagonal B_{36} as a potential basis for extended single-atom layer boron sheets. *Nat. Commun.* **2014**, *5*, 3113. [CrossRef]
12. Gonzalez Szwacki, N.; Sadrzadeh, A.; Yakobson, B.I. B_{80} Fullerene: An Ab Initio Prediction of Geometry, Stability, and Electronic Structure. *Phys. Rev. Lett.* **2007**, *98*, 166804. [CrossRef]
13. Zhai, H.J.; Zhao, Y.F.; Li, W.L.; Chen, Q.; Bai, H.; Hu, H.S.; Piazza, Z.A.; Tian, W.J.; Lu, H.G.; Wu, Y.B.; et al. Observation of an all-boron fullerene. *Nat. Chem.* **2014**, *6*, 727–731. [CrossRef]
14. Gonzalez Szwacki, N. Boron Fullerenes: A First-Principles Study. *Nanoscale Res. Lett.* **2007**, *3*, 49. [CrossRef]
15. Chernozatonskii, L.A.; Sorokin, P.B.; Yakobson, B.I. New boron barrelenes and tubulenes. *JETP Lett.* **2008**, *87*, 489–493. [CrossRef]
16. Singh, A.K.; Sadrzadeh, A.; Yakobson, B.I. Probing Properties of Boron α-Tubes by Ab Initio Calculations. *Nano Lett.* **2008**, *8*, 1314–1317. [CrossRef]
17. Yang, X.; Ding, Y.; Ni, J. *Ab initio* prediction of stable boron sheets and boron nanotubes: Structure, stability, and electronic properties. *Phys. Rev. B* **2008**, *77*. [CrossRef]
18. Tang, H.; Ismail-Beigi, S. First-principles study of boron sheets and nanotubes. *Phys. Rev. B* **2010**, *82*. [CrossRef]
19. Gonzalez Szwacki, N.; Tymczak, C. The symmetry of the boron buckyball and a related boron nanotube. *Chem. Phys. Lett.* **2010**, *494*, 80–83. [CrossRef]
20. Gunasinghe, R.N.; Kah, C.B.; Quarles, K.D.; Wang, X.Q. Dispersion corrections in the boron buckyball and nanotubes. *Appl. Phys. Lett.* **2011**, *98*, 261906. [CrossRef]
21. Kunstmann, J.; Bezugly, V.; Rabbel, H.; Rümmeli, M.H.; Cuniberti, G. Unveiling the Atomic Structure of Single-Wall Boron Nanotubes. *Adv. Funct. Mater.* **2014**, *24*, 4127–4134. [CrossRef]
22. Caliskan, E.; Kirca, M. Tensile characteristics of boron nanotubes by using reactive molecular dynamics simulations. *Comput. Mater. Sci.* **2022**, *209*, 111368. [CrossRef]
23. Kondo, T. Recent progress in boron nanomaterials. *Sci. Technol. Adv. Mater.* **2017**, *18*, 780–804. [CrossRef] [PubMed]
24. Dieb, T.M.; Ju, S.; Shiomi, J.; Tsuda, K. Monte Carlo tree search for materials design and discovery. *MRS Commun.* **2019**, *9*, 532–536. [CrossRef]
25. Paszkowicz, W. Genetic Algorithms, a Nature-Inspired Tool: Survey of Applications in Materials Science and Related Fields. *Mater. Manuf. Process.* **2009**, *24*, 174–197. [CrossRef]
26. Davies, T.E.B.; Popa, M.M.; Ciobanu, C.V.; Maroulis, G.; Simos, T.E. Genetic Algorithm for Structural Optimization of Tubular Nanostructures. *AIP Conf. Proc.* **2007**, *963*, 168. [CrossRef]
27. Tang, H.; Ismail-Beigi, S. Novel Precursors for Boron Nanotubes: The Competition of Two-Center and Three-Center Bonding in Boron Sheets. *Phys. Rev. Lett.* **2007**, *99*, 115501. [CrossRef]
28. Tarkowski, T.; Gonzalez Szwacki, N. The structure of thin boron nanowires predicted using evolutionary computations. *arXiv* **2022**, arXiv:2211.11901. [CrossRef]
29. Tarkowski, T. Quilë. 2022. Available online: https://doi.org/10.5281/zenodo.6484743 (accessed on 9 November 2022).
30. Tarkowski, T.; Gonzalez Szwacki, N.; Marchwiany, M. Structure of porous two-dimensional boron crystals. *Phys. Rev. B* **2021**, *104*, 195423. [CrossRef]
31. Tarkowski, T.; Majewski, J.A.; Gonzalez Szwacki, N. Energy decomposition analysis of neutral and negatively charged borophenes. *FlatChem* **2018**, *7*, 42–47. [CrossRef]
32. Hernández, E.; Goze, C.; Bernier, P.; Rubio, A. Elastic properties of single-wall nanotubes. *Appl. Phys. A* **1999**, *68*, 287–292. [CrossRef]
33. Umari, P.; Petrenko, O.; Taioli, S.; Souza, M.M.D. Communication: Electronic band gaps of semiconducting zig-zag carbon nanotubes from many-body perturbation theory calculations. *J. Chem. Phys.* **2012**, *136*, 181101. [CrossRef]
34. Planck Collaboration; Aghanim, N.; Akrami, Y.; Ashdown, M.; Aumont, J.; Baccigalupi, C.; Ballardini, M.; Banday, A.J.; Barreiro, R.B.; Bartolo, N.; et al. Planck 2018 results—VI. Cosmological parameters. *Astron. Astrophys.* **2020**, *641*, A6. [CrossRef]

35. Hoffmann, R.; von Ragué Schleyer, P.; Schaefer, H.F., III. Predicting Molecules–More Realism, Please! *Angew. Chem. Int. Ed.* **2008**, *47*, 7164–7167. [CrossRef]
36. AMD CPU. Available online: https://www.amd.com/en/product/8436 (accessed on 9 November 2022).

Disclaimer/Publisher's Note: The statements, opinions and data contained in all publications are solely those of the individual author(s) and contributor(s) and not of MDPI and/or the editor(s). MDPI and/or the editor(s) disclaim responsibility for any injury to people or property resulting from any ideas, methods, instructions or products referred to in the content.